Absorption, Magnetic Circular Dichroism, IR Spectra, Electrochemistry, and Molecular Orbital Calculations of Monoaza- and Opposite Diazaporphyrins

Hiroshi Ogata,[a] Takamitsu Fukuda,[a] Katsunori Nakai,[a] Yuichi Fujimura,[a] Saburo Neya,[b] Pavel A. Stuzhin,[c] and Nagao Kobayashi*[a]

Keywords: Cyclic voltammetry / Density functional calculations / Magnetic circular dichroism / Porphyrinoids / UV/Vis spectroscopy

Electronic absorption, magnetic circular dichroism (MCD), IR spectra, and cyclic and differential pulse voltammograms of metal-free and copper monoaza- and opposite diazaporphyrins are reported, together with molecular orbital (MO) calculations using the density functional theory (DFT) method. Introduction of nitrogen atoms at the *meso* position of porphyrins caused a blue-shift of the B band and a red-shift of the Q band, with a concomitant decrease and increase of the apparent absorption coefficient, respectively. On going from monoaza to diaza species, the apparent bandwidth at half-height of the B band and the splitting of the Q band do not change significantly for metal-free species, but increase for the copper species. The MCD peaks and troughs correspond closely to the peaks of the absorption spectra, so that these are interpreted as the superimposition of Faraday *B* terms. The MCD sign pattern (minus-to-plus on going from longer to shorter wavelengths) substantiates experimentally that the splitting between the HOMO and HOMO–1 orbital is larger than that between the LUMO and LUMO+1. Of the copper complexes of octaethylporphyrin (OEP), monoaza- (MAP), diaza- (DAP) and tetraazaporphyrins (TAP), CuTAP is the easiest to reduce and hardest to oxidize. The potential differences between the first oxidation and reduction couples were about 2.1–2.4 V. MO calculations using DFT succeeded in reproducing some of the above spectroscopic and electrochemical characteristics. In addition, some of the IR bands were assigned on the basis of the DFT calculations.

Introduction

Azaporphyrins (APs) are porphyrins whose *meso*-carbon atoms have been replaced by nitrogen atoms to a varying degree. Monoaza- (MAP)[1−3] and diaza-porphyrins (DAP)[4] were first synthesized in the second half of the 1930s, and since then their improved synthesis,[5−13] and electronic absorption,[14−18] fluorescence,[19−21] IR,[6,16] NMR,[6,9,14−16,22] and EPR[15,16,23] spectra have been reported. While the spectroscopic changes due to the introduction of nitrogen atom(s) have often attracted the attention of physical chemists, to date no-one has applied magnetic circular dichroism (MCD) to these species. MCD spectroscopy[24] provides ground- and excited-state degeneracy information, which is needed to fully understand the electronic structure of high symmetry molecules. We, therefore, have applied this spectroscopy to various phthalocyanine (Pc)[25] and low symmetry Pc derivatives[26] and confirmed its utility in analyzing the electronic structure of these large aromatic metallocomplexes. In addition, no-one has attempted to interpret the IR spectra of these low-symmetry compounds by quantum mechanical calculations either. Electrochemical data on APs have also been rarely reported; the first oxidation potentials of a few MAPs in butyronitrile[16] and the first reduction potentials of MAP- and DAP-reconstituted hemoproteins[27] were recorded in a tris-buffer solution. Accordingly, no oxidation and reduction potentials have been reported for single AP derivatives. We therefore report here the electronic absorption, MCD and IR spectra, and electrochemistry of metal-free and copper MAP and DAP, together with results of quantum mechanical calculations.

[a] Department of Chemistry, Graduate School of Science, Tohoku University,
Sendai 980−8578, Japan
Fax: (internat.) +81-22-217-7719
E-mail: nagaok@mail.tains.tohoku.ac.jp
[b] Department of Physical Chemistry, Graduate School of Pharmaceutical Science, Chiba University,
Inage-Yayoi, Chiba 263−8522, Japan
[c] Ivanovo State Academy for Chemistry and Technology
pr. F. Engel'sa 7, 153460, Russia

Results and Discussion

Electronic Absorption and MCD Spectroscopy

Figure 1 denotes the structures of the monoaza and diaza species used in this study. Figure 2 and 3 the show absorp-

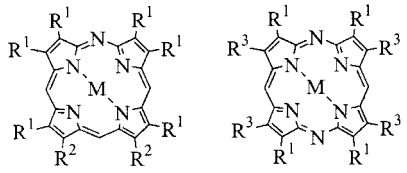

MAP DAP

H_2MAP M = H_2 $R^1 = CH_3$ $R^2 = CH_2CH_2CO_2CH_3$

CuMAP M = Cu $R^1 = CH_3$ $R^2 = CH_2CH_2CO_2CH_3$

H_2DAP M = H_2 $R^1 = CH_3$ $R^3 = C_4H_9$

CuDAP M = Cu $R^1 = CH_3$ $R^3 = C_4H_9$

Figure 1. Structures and abbreviations of the monoaza- (MAP) and diazaporphyrins (DAP) used in this study

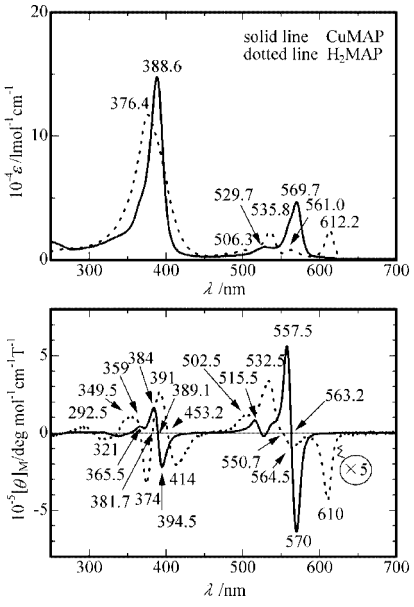

Figure 2. Electronic absorption (top) and MCD (bottom) spectra of CuMAP (solid lines) and H_2MAP (dotted lines) in chloroform; note the encircled magnification factor for the MCD of H_2MAP

tion and MCD spectra of the monoaza and diaza species, respectively.

Metal-Free Species

In the case of H_2MAP (Figure 2), the Q_{x00} and Q_{y00} bands appear at 612 and 536 nm, respectively. The wavelength of the former band is shorter than that of octaethylporphyrin (OEP)[28] by about 10 nm, while that of the latter is slightly longer by several nanometers. The splitting energy between the Q_{x00} and Q_{y00} bands is about 2320 cm^{-1}. The B band appears at 376 nm, which is shorter than that of OEP by more than 20 nm, while its shape is not symmetrical and the bandwidth is apparently larger than that of OEP. In H_2DAP, the two Q bands are red-shifted by about 11 nm, with a splitting energy of 2280 cm^{-1}, and are slightly more intense than in H_2MAP. The B band is only slightly blue-shifted, and the apparent absorption coefficient decreases.

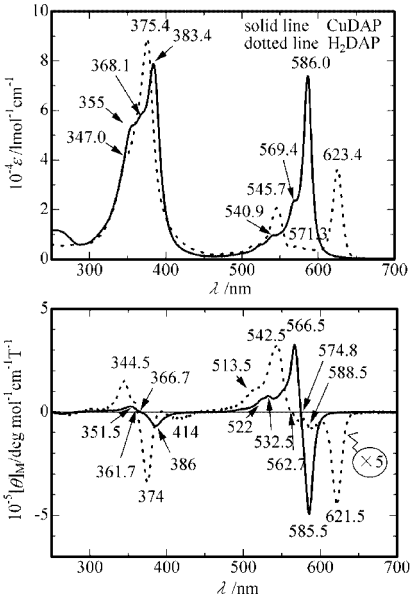

Figure 3. Electronic absorption (top) and MCD (bottom) spectra of CuDAP (solid lines) and H_2DAP (dotted lines) in chloroform; note the encircled magnification factor for the MCD of H_2DAP

The MCD peaks and troughs are observed roughly in the same positions as the absorption peaks and shoulders (Faraday *B* terms). In the Q-band region, the first and third peaks from the lower-energy side correspond to the Q_{x00} and Q_{y00} band for both H_2MAP and H_2DAP, since they show opposite signs. In the B region of H_2MAP, two dispersion curves appear, corresponding to the broad absorption spectra. These are considered to be due to pseudo-Faraday *A* terms produced by superimposition of at least four closely lying Faraday *B* terms.[30] In the B MCD of H_2DAP, the complexity of the spectra on the longer-wavelength side observed for H_2MAP decreases, and the most intense MCD trough and peak in this region appear to correspond to the absorption peak and shoulder, respectively.

Copper Species

The most intense Q- and B-band peaks of CuMAP appear at 570 and 389 nm, respectively. Since the corresponding bands of CuOEP occur at 560 and 399 nm, respectively,[28] the Q- and B-bands are shifted by about 10 nm to the red and blue, respectively, on introduction of one *meso*-nitrogen atom. In the case of CuDAP, the Q-band shifts further, to 586 nm, with an increase in intensity, while the B-band shifts to the blue, to 383 nm, with a loss of intensity. The apparent ratio of the absorption coefficient of the B-band to that of the Q-band [ε(B)/ε(Q)] decreases from about 12. 4 for CuOEP[28] to about 3.2 for CuMAP and further to about 1.1 for CuDAP, indicating that the Q-band becomes more intense with an increasing number of *meso*-nitrogen atoms.[29] In addition, the B-band is significantly broader than with CuMAP.

CuMAP shows dispersion-type MCD curves corresponding to the most intense Q- and B-band peaks. However,

these are considered to be pseudo-Faraday *A* terms produced by two *B* terms of opposite sign.[30] The MCD trough at 570 nm coincides with the absorption maximum, while the MCD peak at 558 nm corresponds to an absorption shoulder seen at the shorter-wavelength side of the absorption peak at 570 nm. The wavelength of the inflection point of the B MCD matches the absorption peak wavelength. These apparent *A* terms are produced, since the degeneracy of the LUMO is not lifted markedly by introduction of one *meso*-nitrogen atom. The Q MCD of CuDAP also has a dispersion-type curve. However, these are also Faraday *B* terms, since the Q MCD trough at 586 nm and the peak at 567 nm correspond closely to the absorption peaks at 586 and 569 nm, respectively. This feature is more clearly seen in the B MCD curve, which is weaker than that of CuMAP. The MCD trough and peak at 386 and 352 nm closely correspond to absorption peaks at 383 and 355 nm, respectively, and the shape of the inflection point is not as clear as for the Q band, indicating a significant splitting of the Soret band. Since both CuMAP and CuDAP display a negative-to-positive MCD pattern, it is experimentally suggested that the splitting of the LUMO is smaller than that between the HOMO and HOMO−1.[31]

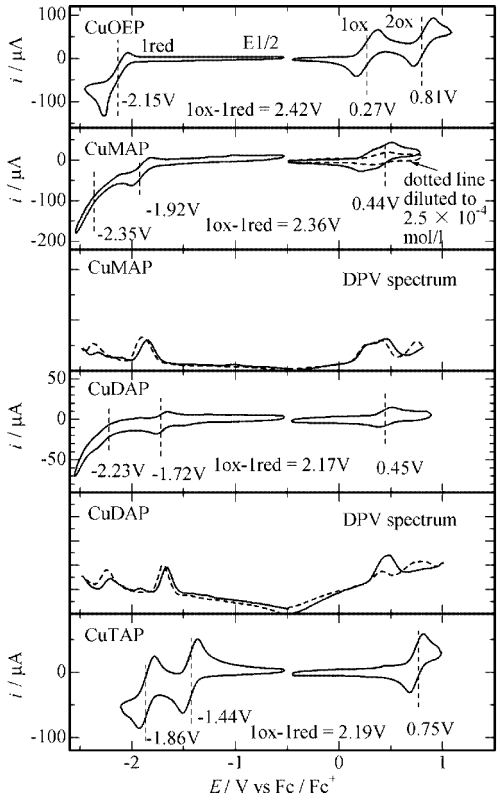

Figure 4. Cyclic and differential pulse voltammograms of CuOEP, CuMAP, CuDAP (opposite type), and CuTAP (from top to bottom) in *o*-DCB containing 0.1 mol/L TBAP

Electrochemistry

As described in the introductory portion, electrochemical data on MAP and DAP are still very rare, and even the first oxidation and reduction potentials of a single azaporphyrin derivative are not known. We therefore recorded the cyclic and differential pulse voltammograms of CuTAP and CuDAP, together with the CV curves of CuOEP and CuTAP in *o*-dichlorobenzene (*o*-DCB) (Figure 4). In the order OEP, MAP, DAP, and tetraazaporphyrin (TAP) — with increasing number of *meso*-nitrogen atoms — the first oxidation potential becomes more positive, since *meso*-nitrogen atoms withdraw electrons from the core of the skeleton, as follows: 0.27, 0.44, 0.45, 0.75 V, respectively. Similarly the first reduction potential varies as −2.15, −1.92, −1.72, −1.44 V, respectively, while the second reduction potential varies as (unmeasureable), −2.35, −2.23, −1.86 V, respectively. The potential difference between the first oxidation and reduction potentials of OEP derivatives is known to be 2.25 ± 0.15 V.[32] These values for CuMAP, CuDAP, and CuTAP are 2.36, 2.17, and 2.19 V, respectively, indicating that the introduction of *meso*-nitrogen atoms does not significantly affect the values. The slightly smaller value for CuDAP (2.17 V) is related to the appearance of the Q-band at longer wavelength due to its D_{2h} symmetry. The potential differences between the first and second reduction potentials for these species are 0.43, 0.51, and 0.42 V, respectively, in the above order, versus 0.42 ± 0.05 V reported for OEP derivatives.[32] These properties can be reproduced by MO calculations, as described in the next section.

MO Calculations

Orbital Energy

Molecular orbital calculations on a series of compounds between normal porphyrins and *meso*-azaporphyrins using CNDO/S Hamiltonian have been reported by Solovyov et al.[19,33] Important differences were found in the energies of the HOMOs between our results and those of Solovyov et al. Diamagnetic zinc was employed instead of paramagnetic copper as the central metal. As shown in Figure 5, the HOMO energy stabilizes moderately in contrast to almost no change reported by Solovyov et al., although the HOMO−1 orbital stabilizes significantly with increasing number of *meso*-nitrogen atoms, since this orbital has a large coefficient at the *meso* positions, as a_{2u} orbitals in D_{4h}-symmetric porphyrins and Pcs.

The LUMO also generally stabilizes with increasing number of *meso*-nitrogen atoms. Accordingly, these trends are in agreement with the observation (Figure 4) that both the first oxidation and reduction potentials become more positive with the introduction of *meso*-nitrogen atoms. As a result, the calculated energy differences between the HOMO and LUMO decrease in the order of OEP (3.027), MAP (2.939), DAP (2.690), and TAP (2.681 V), illustrating a good relationship with the experimental energy difference

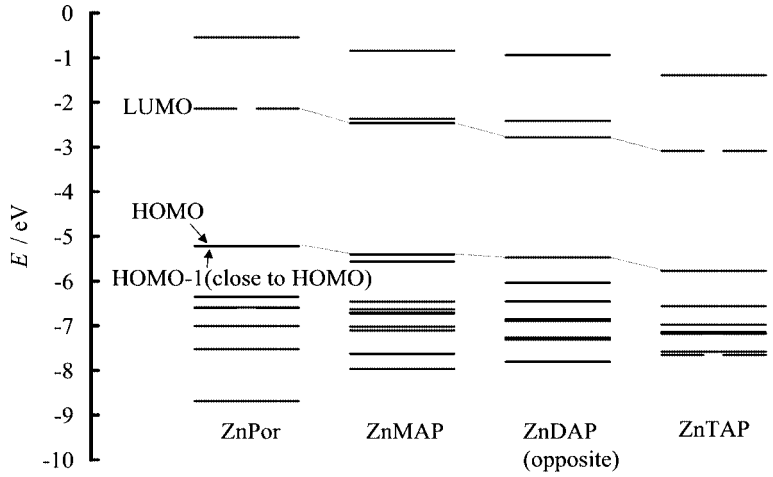

Figure 5. Partial energy diagram for ZnOEP, ZnMAP, ZnDAP (opposite type), and ZnTAP (left to right)

Table 1. Calculated transition energies, oscillator strength (*f*), and configurations for zinc monoaza- and opposite diazaporphyrins[a]

Energy (eV)	Wavelength (nm)	*f*	Configurations (coefficients of the wave function for each excitation)	Angles (°)[b]
ZnMAP				
2.430	510.3	0.0044	95→97 (0.5121) 94→96 (0.5025)	0
2.449	506.2	0.0215	95→96 (0.5343) 94→97 (−0.4661)	90
3.490	355.3	0.6457	95→97 (0.3444) 94→96 (−0.3334) 92→97 (0.2477) 88→96 (−0.1783) 91→97 (−0.1667)	0
3.498	354.5	0.0525	92→96 (0.5947) 90→97 (0.2365) 91→96 (0.1715) 94→97 (0.1240)	90
3.520	352.2	0.6269	94→97 (0.3565) 95→96 (0.3012) 92→96 (−0.2421) 91→96 (0.2392) 88→97 (0.1646)	90
3.583	346.0	0.0607	90→96 (0.5124) 92→97 (0.3765) 91→97 (0.1891) 94→96 (0.1086)	180
3.647	340.0	0.1571	91→96 (0.5952) 94→97 (−0.2086) 92→96 (−0.1242) 95→96 (−0.1216) 90→97 (0.1071)	90
3.736	331.9	0.1477	92→97 (0.4178) 91→97 (−0.4145) 90→96 (−0.2449) 94→96 (0.1613) 95→97 (−0.1175)	180
4.089	303.3	0.2050	88→96 (0.6634)	0
4.197	295.4	0.1484	88→97 (0.5224) 95→98 (−0.3885) 87→96 (0.1661)	90
ZnDAP				
2.457	504.7	0.1190	95→96(0.5741) 94→97(0.3740)	0
2.479	500.2	0.0119	95→97(0.5291) 94→96(−0.4899)	90
3.422	362.3	0.0430	92→96(0.6666) 94→97(0.1017)	180
3.594	344.9	0.5989	94→96(0.3587) 95→97(0.3190) 88→96(0.3047) 92→97(0.1938)	90
3.763	329.5	0.7029	94→97(0.5144) 95→96(−0.2055) 92→96(−0.1561) 88→97(0.1405)	180
3.833	323.5	0.1535	92→97(0.6255) 94→96(−0.1765) 95→97(−0.1123)	90
3.972	312.1	0.3136	88→96(0.6100) 92→97(−0.2068) 94→96(−0.1405) 95→97(−0.1251)	90
4.304	288.1	0.1821	88→97(0.6713) 94→97(−0.1052)	0
5.360	231.3	0.0697	91→98(0.6890)	0
5.387	230.1	0.0530	90→98(0.6896)	90

[a] MO number 95 is the HOMO. Excited states with energy less than ca. 5.4 eV and *f* greater than 0.04 are shown (first and second transitions are included, although some *f* values are smaller than 0.04). [b] Angles between dipole moments of the first and higher electronic transitions (°).

between the first oxidation and reduction potentials (2.36, 2.17, and 2.19 V for CuMAP, CuDAP, and CuTAP, respectively). In addition, as suggested experimentally by a negative-to-positive MCD pattern for CuMAP and CuDAP, the calculated splitting between the HOMO and HOMO−1 is larger than that between the LUMO and LUMO+1 in these molecules. Thus, the calculated MO energies reproduce well the redox properties and one aspect of the MCD spectra.

Calculated Spectra

Table 1 summarizes the calculated absorption data of ZnMAP and ZnDAP. Not all the spectroscopic properties have been satisfactorily reproduced. However, the following results do reproduce the experimental trends. 1) The Q-band splitting is very small (less than 5 nm, ca. 150−180 cm^{-1}), as is discernible from the MCD of CuMAP and CuDAP (Figure 2 and 3). 2) The Q-band intensity is larger for the DAP species than for MAP. 3) Of the split Q-band, the one at longer wavelength is much stronger than that at shorter wavelength for the DAP species, as seen for CuDAP. 4) The purity of the Q-band increases with increasing number of *meso*-nitrogen atoms, since the energy difference between the HOMO and HOMO−1 increases. 5) The positions of the split Soret bands of DAP appear at shorter wavelength while their splitting is larger than for the MAP species. Judging from their configuration and intensity, the bands at 355 and 352 nm are the split Soret bands of ZnMAP, while the Soret bands of ZnDAP were estimated at 345 and 330 nm. On the other hand, the calculated features that do not agree with the experiments are as follows. 1) The Q-bands of the MAP species were calculated at slightly longer wavelength (510 and 506 nm) than those of the DAP species (505 and 500 nm). 2) Of the Q-bands of the MAP species, the band at longer wavelength is weaker than that at shorter wavelength. Thus, the calculations are able to roughly reproduce many of the experimental trends.

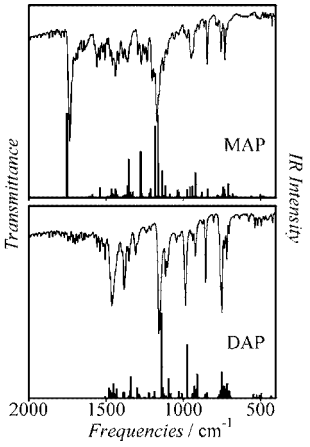

Figure 6. Experimental and calculated (bars) IR spectra of CuMAP (top) and CuDAP (bottom); in the calculation, Cu atoms were replaced by Zn

Structural Modelling and IR Spectra

Although the vibrational structures of tetraazaporphyrins (TAPs) and porphyrins (Pors) are expected to be similar because of the close resemblance of their skeletons, some differences were still detected between the experimental IR spectra of MAP and DAP, as depicted in Figure 6. One of the reasons for this obviously arises from the different substituents at the β-positions of the pyrroles. In order to eliminate the substituent effects and allow comparison of the IR spectra of MAP and DAP, quantum chemical calculations may be helpful. Accordingly, DFT calculations of IR spectra of MAP and DAP using the B3LYP[34] functional in combination with the 6−31G(d) basis set were performed, since this combination has been previously demonstrated to satisfactorily reproduce the experimental IR spectra of low symmetrical tetraaza-chlorin, bacteriochlorin, and isobacteriochlorin derivatives.[35,36] For simplicity of calculations, diamagnetic zinc was employed instead of paramagnetic copper as the central metal.

Table 2. Comparison of selected geometric parameters between ZnMAP and ZnDAP

ZnMAP		ZnDAP	
N5−C9	1.331	N5−C9	1.331
N5−C10	1.331	N5−C10	1.331
		N6−C1	1.331
		N6−C18	1.331
C5−C6	1.388	C5−C6	1.399
C5−C4	1.405	C5−C4	1.399
C14−C13	1.388	C14−C13	1.399
C14−C15	1.405	C14−C15	1.399
C19−C1	1.397		
C19−C18	1.397		
C2−C3	1.376	C2−C3	1.372
C7−C8	1.368	C7−C8	1.372
C11−C12	1.368	C11−C12	1.372
C16−C17	1.376	C16−C17	1.372
N1−N2	2.874	N1−N2	2.860
N2−N3	2.806	N2−N3	2.809
N3−N4	2.874	N3−N4	2.860
N4−N1	2.889	N4−N1	2.809
C9−N5−C10	123.4	C9−N5−C10	124.0
		C1−N6−C18	124.0
C4−C5−C6	126.9	C4−C5−C6	127.1
C13−C14−C15	127.0	C13−C14−C15	127.1
C18−C19C1	127.5		

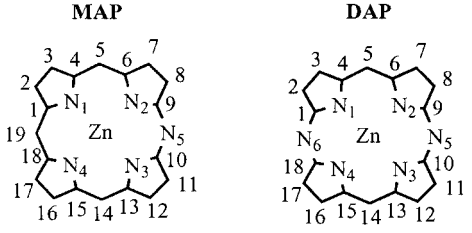

Figure 7. Positions of atoms used in calculating frequencies, ZnMAP (left) and ZnDAP (right)

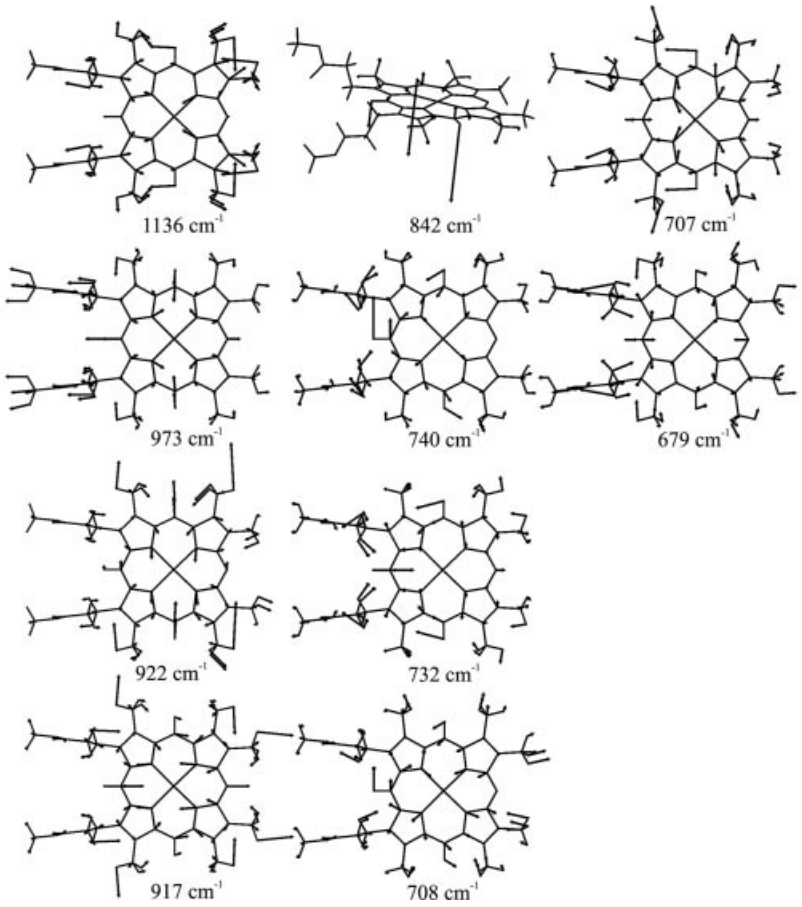

Figure 8. Atomic movements at the selected predicted frequencies of ZnMAP

MAP and DAP have planar skeletal structures with C_{2v} and D_{2h} symmetry, respectively. Table 2 presents selected bond lengths and angles obtained from the calculations (see also Figure 7). The lengths of the C−C and C−N bonds are 1.368−1.405 and 1.331 Å, respectively, which are within the typical values of aromatic compounds, implying a lack of strain in the molecules. The C−C−C and C−*N*−C angles are also normal. The $N_{pyrrole}-N_{pyrrole}$ distances across the azamethine group (i.e. N2−N3 for MAP and N2−N3 and N4−N1 for DAP) are shorter than the other $N_{pyrrole}-N_{pyrrole}$ distances (across the $C-H_{meso}$ group). This is simply because of the larger $C-C_{meso}-C$ bond angles than for the $C-N_{meso}-C$, and the central metal is, therefore, surrounded by the C_{2v}- and D_{2h}-type ligands, respectively.

The calculated harmonic vibrational frequencies (bars) are also listed in Figure 6. The calculated modes were assigned to experimental bands on the basis of both the frequency and intensity data. Some assignable vibrational modes are illustrated in Figure 8 and 9 using vector models. As shown, the correspondence between the experimental and calculated values is good, in particular in the energy region below 1200 cm^{-1}. An intense band at 1753 cm^{-1} for MAP obviously originates from the C=O stretching of the substituted esters. The other skeletal vibrations appear below about 1500 cm^{-1}. The out-of-plane motion of the hydrogens appears in the energy region below about 1000 cm^{-1}. In particular, the out-of-plane motion of the $C-H_{meso}$ groups was assigned to the peaks at 842 and 846 cm^{-1} for MAP and DAP, respectively, which demonstrates an independence of this type of vibration of the molecular structures. Although the intense bands at 1180 and 1163 cm^{-1} (MAP) and 1140 cm^{-1} (DAP) are energetically close, the former two bands originate from vibrations localized on the substituents, and the latter from inner skeletal vibrational modes. The effect of substituents was characterized by relatively intense bands. The in-plane motions of the skeleton are located at 1136, 973, 922, 917, 740, and 732 cm^{-1} for MAP and at 1340, 1132, 1094, 973, 928, 917, 910, 749, and 734 cm^{-1} for DAP. The above results illustrate that the DFT calculations are able to satisfactorily reproduce the experimental IR spectra.

Conclusion

Electronic absorption, MCD, and IR spectra, and redox potentials of metal-free and copper monoaza- and opposite diazaporphyrins have been reported, together with their molecular orbital (MO) and vibrational frequencies on the

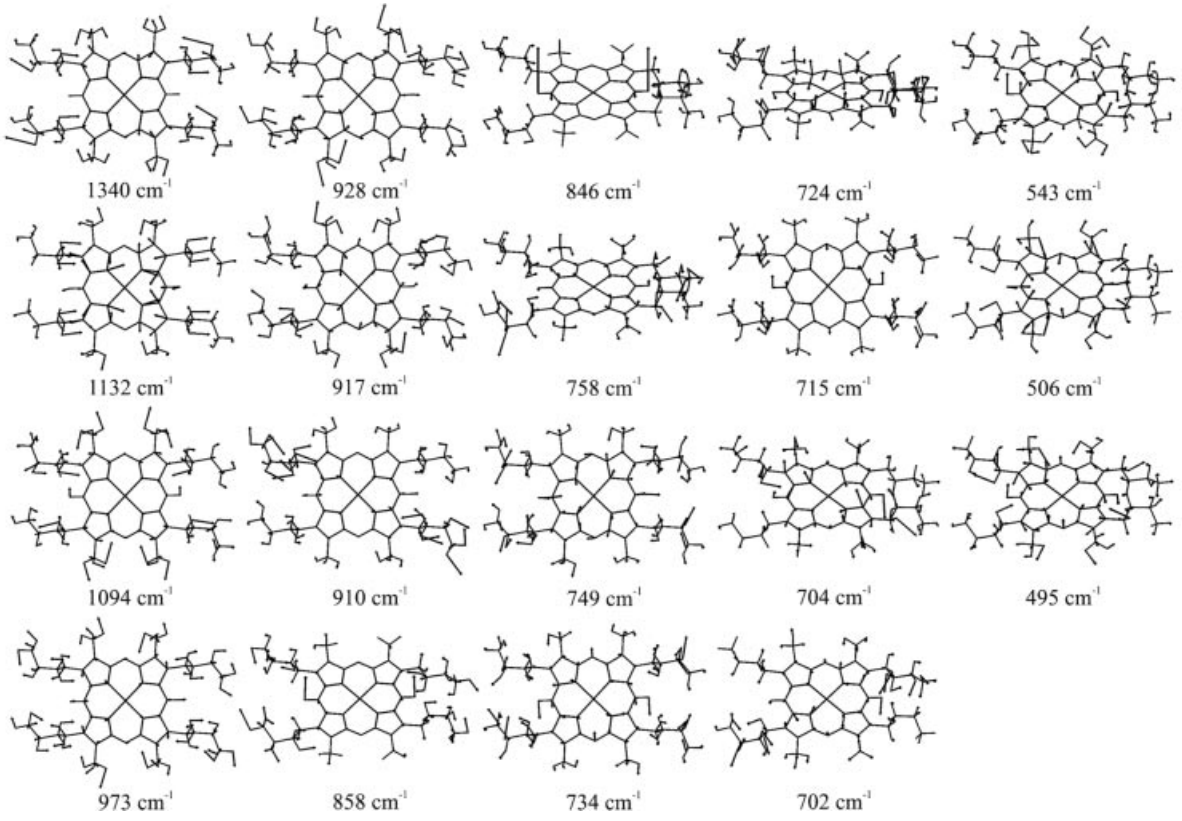

Figure 9. Atomic movements at the selected predicted frequencies of ZnDAP

basis of DFT calculations. The introduction of nitrogen atoms at the *meso* position of the porphyrins causes a blue-shift of the B-band and a red-shift of the Q-band with concomitant decrease and increase, respectively, of the apparent absorption coefficient. However, the bandwidth of the B-band and the splitting of the Q-band do not change systematically with the number of *meso*-nitrogen atoms. On going from monoaza to diaza species, the apparent bandwidth at half-height of the B-band and the splitting of the Q-band do not change significantly for metal-free species, although they increase for the copper species. All MCD curves are interpreted as the superimposition of Faraday *B* terms, since there is no orbital degeneracy in the excited states. The MCD sign pattern (minus-to-plus on going from longer to shorter wavelengths) substantiates experimentally that the splitting between the HOMO and HOMO−1 orbital is larger than that between the LUMO and LUMO+1. Of the copper complexes of octaethylporphyrin (OEP), monoaza- (MAP), diaza- (DAP) and tetraazaporphyrins (TAP), the first oxidation becomes more difficult, while the first reduction becomes easier with increasing number of *meso* nitrogen atoms. The potential differences between the first oxidation and reduction couples are about 2.1−2.4 V. MO calculations using DFT succeeded in reproducing some of the above spectroscopic and electrochemical characteristics. In addition, the good correspondence between the DFT calculations and experimental data enabled some IR bands to be assigned.

Experimental Section

Measurements: Mass spectra were obtained using a Micromass LCT Spectrometer (ESI-TOF mass). Electronic absorption spectra were recorded with a Hitachi U-3410 spectrophotometer using chloroform as solvent. Magnetic circular dichroism (MCD) measurements were made with a JASCO J-725 spectrophotometer equipped with a JASCO electromagnet that produces magnetic fields of up to 1.09 T. Its magnitude was expressed in terms of molar ellipticity per tesla, $[\theta]_M$/deg·mol^{-1}·dm^3·cm^{-1}·T^{-1}. IR spectra were recorded on a Shimadzu FTIR-8100M spectrometer using KBr disks. Cyclic voltammetry (CV) and differential pulse voltammetry (DPV) experiments were carried out with conventional three-electrode cells, in which a platinum wire auxiliary electrode, a glassy carbon working electrode (0.07 cm^2), and an Ag/AgCl wire reference electrode were employed. The solvent for electrochemical measurements, *o*-dichlorobenzene (*o*-DCB, Nacalai Tesque, specially prepared for HPLC) was used as supplied. Tetrabutylammonium perchlorate (TBAP) was used as an electrolyte. The ferrocenium/ferrocene (Fc^+/Fc) couple was used as an internal standard. In DCB containing 0.1 M TBAP, the Fc^+/Fc couple was observed at approximately +510 ± 20 mV vs. AgCl/Ag. All electrochemical work was carried out under an atmosphere of dry nitrogen. CV data were collected with a Hokuto Denko HA-501 potentiostat/galvanostat connected to a Hokuto Denko HB-104 function generator and a Graphtec WX1200 XY recorder. DPV data were collected with a Yanaco P-1100 polarographic analyzer connected to a Graphtec WX2400 XY recorder.

Materials: H_2DAP,[13] CuDAP,[12] and CuTAP[37] were synthesized as reported in our previous papers. CuMAP and CuOEP were ob-

tained by reacting H_2MAP[38] or commercially available H_2OEP and $Cu(OAc)_2 \cdot H_2O$ in ethanol/dichloroethane (1:1 v/v) at 80 °C for 18 h, and subsequent purification using an alumina column and chloroform as eluent.

CuOEP: ESI-TOF: calcd. for $C_{36}H_{44}CuN_4$ 596.31; found 595.40. $C_{36}H_{44}CuN_4$ (596.31): calcd. C 72.51, H 7.44, N 9.40, found C 71.24, H 7.52, N 9.17.

CuMAP: ESI-TOF: calcd. for $C_{33}H_{35}N_5O_4Cu$ 629.21; found 629.24. $C_{33}H_{35}N_5CuO_4$ (629.21): calcd. C 62.99, H 5.61, N 11.13, found C 62.26, H 5.63, N 10.78.

Computational Methods: The Gaussian 98 program[39] running on an NEC TX7/AzusA computing system operated by Tohoku University Supercomputing System Information Synergy Center was used to perform DFT calculations of MOs (electron transitions) and frequencies. Since copper is paramagnetic, the central metal was taken to be zinc. B3LYP[34] with the 6−31G(d) basis set was used for all geometry optimization, MOs and frequency calculations. The transition energies and intensities of the lowest 30 singlet-singlet electronic transitions were determined by time-dependent DFT. An optimum scaling factor of 0.9613 was applied to the calculated frequencies in order to compare with the experimental data.[40]

Acknowledgments

This research was partially supported by the Ministry of Education, Science, Sports and Culture, with a Grant-in-Aid for the COE project "Giant Molecules and Complex Systems, 2004".

[1] H. Fischer, W. Friedrich, *Justus Liebigs Ann. Chem.* **1936**, *523*, 154−164.
[2] F. Endermann, H. Fischer, *Justus Liebigs Ann. Chem.* **1939**, *538*, 172−194.
[3] H. Fischer, H. Orth, *Die Chemie des Pyrroles*, Akad. Verlag, Leipzig, **1940**, Vol. II-ii, pp. 408−11.
[4] H. Fischer, H. Harberland, A. Muller, *Justus Liebigs Ann. Chem.* **1935**, *521*, 122−128.
[5] R. L. N. Harris, A. W. Johnson, I. T. Kay, *J. Chem. Soc., C* **1966**, 22−29.
[6] J. Engel, A. Gossauer, A. W. Johnson, *J. Chem. Soc., Perkin Trans. 1* **1978**, 871−875.
[7] A. M. Abeysekera, R. Grigg, J. F. Malone, J. T. King, J. O. Morley, *J. Chem. Soc., Perkin Trans. 2* **1985**, 395−402.
[8] R. K. Pandey, H. Zhou, K. Gerzevske, K. M. Smith, *J. Chem. Soc., Chem. Commun.* **1992**, 183−185.
[9] J. P. Singh, L. Y. Xie, D. Dolphin, *Tetrahedron Lett.* **1995**, *36*, 1567−1570.
[10] W. Metzger, H. Fischer, *Justus Liebigs Ann. Chem.* **1937**, *527*, 1−37.
[11] H. Fischer, A. Muller, *Justus Liebigs Ann. Chem.* **1937**, *528*, 1−8.
[12] O. G. Khelevina, N. V. Chizhova, P. A. Stuzhin, A. S. Semeikin, B. D. Berezin, *Russ. J. Coord. Chem. (Engl. Transl)* **1996**, *22*, 811−814.
[13] O. G. Khelevina, N. V. Chizhova, P. A. Stuzhin, A. S. Semeikin, B. D. Berezin, *Russ. J. Phys. Chem. (Engl. Transl)* **1997**, *71*, 74−78.
[14] S. Saito, H. A. Itano, *J. Chem. Soc., Perkin Trans. 1* **1986**, 1−7.
[15] A. L. Balch, M. M. Olmstead, N. Safari, *Inorg. Chem.* **1993**, *32*, 291−296.
[16] J. H. Fuhrhop, P. Kruger, W. S. Sheldrick, *Justus Liebigs Ann. Chem.* **1977**, 339−359.
[17] R. Grigg, R. J. Hamilton, M. L. Jozefowicz, C. H. Rochester, R. J. Terrell, H. Wickwar, *J. Chem. Soc., Perkin Trans. 2* **1973**, 407−413.
[18] J. A. Clarke, P. J. Dawson, R. Grigg, C. H. Rochester, *J. Chem. Soc., Perkin Trans. 2* **1973**, 414−416.
[19] S. S. Dvornikov, V. N. Knyukshto, V. A. Kuzmitsky, A. M. Shluga, K. N. Solovyov, *J. Lumin.* **1981**, *23*, 373−392.
[20] G. P. Gurinovich, G. N. Sinyakov, A. M. Shulga, *Izv. Akad. Nauk. SSSR. Ser. Fiz.* **1970**, *34*, 620−624.
[21] V. A. Mashenkov, K. N. Solov'ev, A. E. Turkova, N. A. Yushkevich, *Zh. Prikl. Specktrosk.* **1974**, *21*, 73−81.
[22] F. P. Monforts, B. Gerlach, *Tetrahedron Lett.* **1992**, *33*, 1985−1988.
[23] S. Neya, T. Kaku, N. Funasaki, Y. Shiro, T. Iizuka, K. Imai, H. Hori, *J. Biol. Chem.* **1995**, *270*, 13118−13123.
[24] M. J. Stillman, T. Nyokong, in *Phthalocyanines — Properties and Applications* (Ed.: C. C. Leznoff, A. B. P. Lever), VCH, New York, **1989**, Vol.1, Chapter 3, pp 133−289.
[25] [25a] N. Kobayashi, F. Furuya, G. -C. Yug, H. Wakita, M. Yokomizo, N. Ishikawa, *Chem. Eur. J.* **2002**, *8*, 1474−1484. [25b] N. Kobayashi, *Bull. Chem. Soc. Jpn.* **2002**, *75*, 1−19. [25c] Y. -H. TSE, N. Kobayashi, A. B. P. Lever, *Collect. Czech. Chem. Commun.* **2001**, *66*, 338−354. [25d] N. Kobayashi, A. Muranaka, *Chem. Commun.* **2000**, 1855−1856. [25e] N. Kobayashi, A. Muranaka, K. Ishii, *Inorg. Chem.* **2000**, *39*, 2256−2257. [25f] N. Kobayashi, T. Fukuda, D. Lelievre, *Inorg. Chem.* **2000**, *39*, 3632−3637. [25g] N. Kobayashi, R. Higashi, B. C. Titeca, F. Lamote, A. Ceulemans, *J. Am. Chem. Soc.* **1999**, *121*, 12018−12028. [25h] N. Kobayashi, *Chem. Commun.* **1998**, 487−488. [25i] N. Kobayashi, H. Lam, W. A. Nevin, P. Janda, C. C. Leznoff, T. Koyama, A. Monden, H. Shirai, *J. Am. Chem. Soc.* **1994**, *116*, 879−890. [25j] N. Kobayashi, Y. Kobayashi, T. Osa, *J. Am. Chem. Soc.* **1993**, *115*, 10994−10995.
[26] [26a] N. Kobayashi, J. Mack, K. Ishii, M. J. Stillman, *Inorg. Chem.* **2002**, *41*. 5350−5363. [26b] N. Kobayashi, T. Fukuda, *J. Am. Chem. Soc.* **2002**, *124*, 8021−8034. [26c] N. Kobayashi, H. Miwa, V. N. Nemykin,, *J. Am. Chem. Soc.* **2002**, *124*, 8007−8020. [26d] T. Fukuda, J. R. Stork, R. J. Potucek, M. M. Olmstead, B. C. Noll, N. Kobayashi, W. S. Durfee, *Angew. Chem. Int. Ed.* **2002**, *41*, 2565−2568. [26e] H. Miwa, E. A. Makarova, K. Ishii, E. A. Luk'yanets, N. Kobayashi, *Chem. Eur. J.* **2002**, *8*, 1082−1090. [26f] N. Kobayashi, S. Inagaki, V. N. Nemykin, T. Nonomura, *Angew. Chem. Int. Ed.* **2001**, *40*, 2710−2712. [26g] N. Kobayashi, T. Nonomura, K. Nakai, *Angew. Chem. Int. Ed.* **2001**, *40*, 1300−1303. [26h] N. Kobayashi, A. Muranaka, V. N. Nemykin, *Tetrahedron Lett.* **2001**, *42*, 913−915. [26i] V. N. Nemykin, N. Kobayashi, *Chem. Commun.* **2001**, 165−166. [26j] T. Nyokong, F. Furuya, N. Kobayashi, D. Du, W. Liu, J. Jiang, *Inorg. Chem.* **2000**, *39*, 128−135. [26k] J. Mack, N. Kobayashi, C. C. Lezonoff, M. J. Stillman, *Inorg. Chem.* **1997**, *36*, 5624−5634. [26l] N. Kobayashi, M. Togashi, T. Osa, K. Ishii, S. Yamauchi, H. Hino, *J. Am. Chem. Soc.* **1996**, *118*, 1073−1085.
[27] Y. Mie, K. Sonoda, S. Neya, N. Funasaki, I. Taniguchi, *Bioelectrochem. Bionerg.* **1998**, *46*, 175−184.
[28] K. M. Smith, *Porphyrins and Metalloporphyrins*, Elsevier, Holland, **1976**.
[29] CuTAP shows the Soret and Q_{00} band at 339 and 586 nm, respectively, in the same solvent, and this value becomes about 0.6.[37]
[30] [30a] A. Kaito, T. Nozawa, T. Yamamoto, M. Hatano, Y. Orii, *Chem. Phys. Lett.* **1977**, *52*, 154−160. [30b] A. Tajiri, J. Z. Winkler, *Naturforsch.* **1983**, *38a*, 1263−1269.
[31] [31a] J. Michl, *J. Am. Chem. Soc.* **1978**, *100*, 6801−6811. [31b] J. Michl, *J. Am. Chem. Soc.* **1978**, *100*, 6812−6818. [31c] J. D. Keegan, A. M. Stolzenberg, Y. Lu, R. E. Linder, G. Barth, A. Moscowitz, E. Bunnenberg, C. Djerassi, *J. Am. Chem. Soc.* **1982**, *104*, 4305−4317.
[32] J. H. Fuhrhop, K. M. Kadish, D. G. Davis, *J. Am. Chem. Soc.* **1973**, *95*, 5140−5147.
[33] A conceptual explanation on how the LUMO energy changes depending on the number and position of the *meso*-nitrogen atoms has already been reported: K. N. Solovyov, V. A. Mashenkov, T. F. Kachura, *Opt. Spect.* **1969**, *27*, 24−29.

[34] [34a] A. D. Becke, *J. Chem. Phys.* **1993**, *98*, 5648−5652. [34b] C. Lee, W. Yang, R. G. Parr, *Phys. Rev. B* **1988**, *37*, 785−789.

[35] T. Fukuda, E. M. Makarova, E. A. Luk'yanets, N. Kobayashi, *Chem. Eur. J.* **2004**, *10*, 117−133.

[36] E. M. Makarova, T. Fukuda, E. A. Luk'yanets, N. Kobayashi, *submitted*.

[37] N. Kobayashi, H. Miwa, H. Isago, T. Tomura, *Inorg. Chem.* **1999**, *38*. 479−485.

[38] R. K. Pandey, K. R. Gerzevske, H. Zhou, K. M. Smith, *J. Chem. Soc., Perkin. Trans. 1* **1994**, 971−977.

[39] M. J. Frisch, G. W. Trucks, H. B. Schlegel, G. E. Scuseria, M. A. Robb, J. R. Cheeseman, V. G. Zakrzewski, J. A. Montgomery. Jr, R. E. Stratmann, J. C. Burant, S. Dapprich, J. M. Millam, A. D. Daniels, K. N. Kudin, M. C. Strain, O. Farkas, J. Tomasi, V. Barone, M. Cossi, R. Cammi, B. Mennucci, C. Pomelli, C. Adamo, S. Clifford, J. Ochterski, G. A. Petersson, P. Y. Ayala, Q. Cui, K. Morokuma, N. Rega, P. Salvador, D. D. Dannenberg, D. K. Malick, A. D. Rabuck, K. Raghavachari, J. B. Foresman, J. Cioslowski, J. V. Ortiz, A. G. Baboul, B. B. Stefanov, G. Liu, A. Liashenko, P. Piskorz, I. Komaromi, R. Gomperts, R. L. Martin, D. J. Fox, T. Keith, M. A. Al-Laham, C. Y. Peng, A. Nanayakkara, M. Challacombe, P. M. W. Gill, B. Johnson, W. Chen, M. W. Wong, J. L. Andres, C. Gonzalez, M. Head-Gordon, E. S. Replogle, J. A. Pople, *Gaussian 98, Revision A.11.3*, Gaussian, Inc., Pittsburgh, PA, 2002.

[40] M. W. Wong, *Chem. Phys. Lett.* **1996**, *256*, 391−399.

Received November 8, 2003
Early View Article
Published Online March 9, 2004

